IEEE Access
Multidisciplinary | Rapid Review | Open Access Journal

Received April 4, 2020, accepted April 19, 2020, date of publication April 24, 2020, date of current version May 12, 2020.

Digital Object Identifier 10.1109/ACCESS.2020.2990137

A Novel Method for Predicting Tensile Strength of Friction Stir Welded AA6061 Aluminium Alloy Joints Based on Hybrid Random Vector Functional Link and Henry Gas Solubility Optimization

TAHER A. SHEHABELDEEN[1,2], MOHAMED ABD ELAZIZ[3], AMMAR H. ELSHEIKH[4], OSAMA FAROUK HASSAN[5], YAJUN YIN[1], XIAOYUAN JI[1], XU SHEN[1], AND JIANXIN ZHOU[1]

[1]State Key Laboratory of Materials Processing and Die & Mould Technology, Huazhong University of Science and Technology, Wuhan 430047, China
[2]Department of Mechanical Engineering, Faculty of Engineering, Kafrelsheikh University, Kafrelsheikh 33516, Egypt
[3]Department of Mathematics, Faculty of Science, Zagazig University, Zagazig 44519, Egypt
[4]Department of Production Engineering and Mechanical design, Faculty of Engineering, Tanta University, Tanta 31527, Egypt
[5]Mathematics Department, Faculty of Science, Damanhour University, Damanhour 22511, Egypt

Corresponding author: Jianxin Zhou (zhoujianxin@hust.edu.cn)

This work was supported in part by the State Key Laboratory of Special Rare Metal Materials under Contract SKL2018K004j, and in part by the Northwest Rare Metal Materials Research Institute Ningxia Co., Ltd.

ABSTRACT Aluminum alloys have low weldability by conventional fusion welding processes. Friction stir welding (FSW) is a promising alternative to traditional fusion welding techniques for producing high quality aluminum joints. The quality of the welded joints is highly dependent on the process parameters used during welding. In this research, a new approach was developed to predict the process parameters and mechanical properties of AA6061-T6 aluminium alloy joints in terms of ultimate tensile strength (UTS). A new hybrid artificial neural network (ANN) approach has been proposed in which Henry Gas Solubility Optimization (HGSO) algorithm has been incorporated to improve the performance of Random Vector Functional Link (RVFL) network. The HGSO-RVFL model was constructed with four parameters; rotational speed, welding speed, tilt angle, and pin profile. The validity of the model was tested, and it was demonstrated that the HGSO-RVFL model is a powerful technique for predicting the UTS of friction stir welded (FSWD) joints. In addition, the effects of process parameters on UTS of welded joints were discussed, where a significant agreement was observed between experimental results and predicted results which indicates the high performance of the model developed to predict the appropriate welding parameters that achieve optimal UTS.

INDEX TERMS Friction stir welding, 6061Aluminum alloy, tensile strength, artificial neural network, Henry gas solubility optimization, random vector functional link.

I. INTRODUCTION

AA6061 is a precipitation-hardened aluminum alloy. It has a relatively high strength with good toughness and high corrosion resistance. Furthermore, it offers excellent weldability. Therefore, AA6061 has enormous applications, especially in aerospace, automotive, and marine industries [1], [2]. Intensive structural applications of AA6061 such as truck roofs, side panels, and ship bodies require feasible and efficient welding techniques. Conventional fusion welding of aluminum alloys is unsuitable due to creation of intermetallic compounds, oxide layers, hot cracks in molten weld pool which consequently deteriorate the joint mechanical properties such as strength, hardness, toughness, stiffness, and

The associate editor coordinating the review of this manuscript and approving it for publication was Fan Zhang.

ductility [3]. Friction stir welding (FSW) was first introduced by The Welding Institute, United Kingdom, in 1991, as a new joining technique [4], which initially applied for joining aluminum alloys instead of the conventional fusion welding technique [5]. FSW process has been proposed as a solid state welding technique to weld similar, dissimilar, and composite materials [6]–[8]. FSW process has many advantages over conventional fusion welding methods such as avoiding solidification cracks and porosity as well as the absence of parent metal melting which make this method capable of producing defect-free joints with high mechanical properties. Moreover, the rapid progress in FSW associated technologies such as welding machines, tool design, and tool materials is another advantage of FSW over other conventional techniques. FSW has been widely used in car, ship and airplane industries. In a typical FSW process, a non-consumable rotating tool is used to join two adjacent workpieces without melting the workpiece material. The primary motion is provided by rotating the tool, and the feed motion is provided by traversing the tool along the joint line. The tool starts rubbing onto the workpiece surfaces and heat is generated under friction action. The material around the tool is heated up and a softened material zone is formed. The softened material zone is stirred by the rotating tool to create a solid phase weld.

Rajendran *et al.* [9] studied the influence of tool tilt angle (0°-4°) on the strength of friction welded AA2014-T6 aluminum alloy. It was recommended to use tool tilt angle less than 3° to avoid weld joint defects. The optimum shear strength of the joint (14.42 kN) was obtained at tool tilt angle of 2°. Palanivel *et al.* [10] investigated the effect of the tool profile (straight square, tapered square, straight octagon, tapered octagon, and straight hexagon) and its rotational speed (600 rpm, 950 rpm and 1300 rpm) on the tensile strength and microstructure during FSW of two dissimilar aluminum alloys: AA6351-T6 and AA5083-H111 using a tool made of high carbon chromium steel. It was reported that tensile strength of the welded joint is affected by cold work losses in the heat affected zone of the welded workpieces, flow behavior of the softened material, and defects formed in the weld region. The highest tensile strength of the joint (273 MPa) was obtained using straight square tool profile rotated at 950 rpm. This highest tensile strength is less than the ultimate tensile strength of AA6351-T6 and AA5083-H111 by 11.9% and 11.3%, respectively. The effects of tool geometry (cylindrical and conical) on a FSW lap joint made of two dissimilar aluminum alloys (AA 6082-T6 and AA 5754-H22) have been investigated by Costa *et al.* [11]. The use of a conical tool produced similar strengths welds for retreating and advancing sides. Xu *et al.* [12]studied the fracture behavior of a FSW joint made of AA7085 Al alloy aluminum alloy. The tensile strength under a tool rotational speed of 600 rpm decreases by about 33.3% compared with that of base material. Rajakumar *et al.* [13] investigated the effect of rotational speed (900-1800 rpm), traverse speed (20-100 mm/min) and axial tool force (6-10 KN), tool hardness (33-56 HRC), tool shoulder diameter (9-21 mm), and pin diameter (3-7 mm) on the tensile strength of FSWD joints made of AA7075-T6 alloy. The maximum tensile strength of 373 MPa and joint efficiency of 77% were obtained at rotational speed of 1400 rpm, welding speed of 60 mm/min, axial force of 8 kN, tool hardness of 45 HRC, shoulder diameter of 15 mm, and pin diameter of 5 mm. The enhancement in the tensile properties of the welded joints is due to the fine-grained microstructure with no defects and uniformly distributed finer $MgZn_2$ particles.

The selection and control of FSW process parameters is highly required to enhance the quality of FSWD in terms of mechanical properties. Many artificial intelligence methods have been proposed to predict the process response (output) based on some process inputs by establishing prediction models such as Artificial Neural Networks (ANN) and Adaptive Neuro-Fuzzy Inference System (ANFIS).

ANN based modeling is one of the most significant areas of research in recent decades. It is an artificial intelligence-based system that mimics the function, mechanism and structure of the human brain [14]. Complex problems of a nonlinear nature can be modeled using ANN [15]. It is a complex system consists of many neurons that form the main component of the ANN model and generally composed of input, hidden and output layers. The first layer acts as a receiver to the input parameters. Then the data is processed from the input layer in the hidden layer, and the output is finally computed in the output layer, the number of neurons in the first and last layer is equal to the inputs and outputs of the ANN. ANNs are particularly suitable for identifying highly complex nonlinear phenomena and have been widely used in the study of material constitutive relations [16], [17]. ANN has outstanding generalization capabilities in modeling non-linear mathematical problems [18]–[22]. ANN has been proposed to model different welding processes. Andersen *et al.* [23] developed an ANN model to predict the bead shape during arc tungsten gas welding. Nagesh and Datta [24] used ANN for predicting weld bead geometry and penetration in shielded metal-arc welding and in TIG welding of pure aluminum [25]. Sukhomay *et al.* [26] constructed an ANN model to predict the UTS of inert gas-welded plates and the results of the developed model had a better agreement with experimental ones compared with those obtained by multiple regression analysis. Palanivel *et al.* [27] established an ANN model to predict the UTS of FSWD titanium tubes and compared the results with RSM, and concluded that ANN produced the most accurate predictions. Dehabadi *et al.* [28] used the same technique to predict the microhardness of FSWD AA6061 joints. ANN was also applied to predict the mechanical properties of FSWD aluminum plates including hardness, strength, and elongation [29]. Recently, various metaheuristic optimization algorithms, such as genetic algorithms, particle swarm optimization, artificial bee colony, cat swarm optimization, Harris hawks optimization, and whale optimization algorithm, have been integrated with ANN to determine the optimal ANN structure and parameters [15], [30]–[35].

Genetically optimized neural network systems have been applied to model FSW process. It has been used to search the optimized parameters of the FSW process [36]. Furthermore, the hybrid multi-objective optimization has been applied to improve the microstructural and mechanical properties of B4C/A356 composites fabricated by FSP [37], and aluminum composites reinforced with different reinforcing particles type [38]. Additional studies on ANN applications to model FSW process have been carried out [29], [36], [39]–[42]. Since the FSW process has many variables, which makes it difficult to reach the appropriate parameters that achieve the best results, therefore this work focuses on predicting the optimal output by specifying the appropriate parameters for the welding process to obtain the best mechanical properties. In this study, a new approach to predict UTS of AA6061-T6 FSWD joints is presented. The proposed approach is constructed by integrating ANN with a new metaheuristic algorithm called Henry gas solubility optimization (HGSO) [43] to improve the performance of the Random Vector Functional Link (RVFL) that used to predict the UTS of the FSWD joints under different welding parameters. The use of RVFL avoids the problem that faces the traditional ANN such as overfitting since RVFL connects the input data with the output which improves the prediction accuracy of the output. Moreover, HGSO helps to obtain the optimal RVFL parameters that maximize the prediction accuracy of the model.

II. PROPOSED APPROACH

A. RANDOM VECTOR FUNCTIONAL LINK

In the last decades, the single layer feed forward neural network (SLFNN) has been extended to other more versions, for example, in 1994, Pao *et al.* [44] supposed the Random Vector Functional Link Network, noted as RVFL. The main difference between them that in the RVFL, the input layer and output layer are connected to each other directly, as shown in Fig.1. Such connection can assist the RVFL network to be able to avert the problems of overfitting.

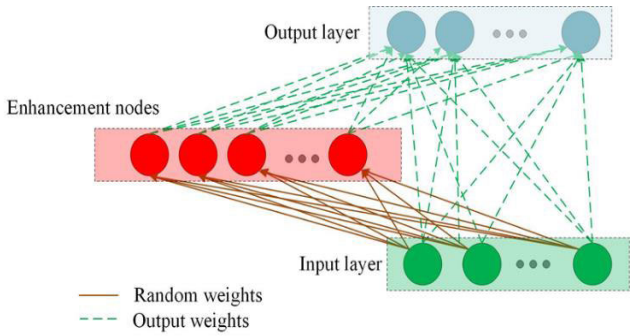

FIGURE 1. The structure of RVFL network.

The RVFL network can be mathematically modeled as following, there is a number N of data samples, where each sample can be symbolized as (x_i, y_i), where $x_i \in R^n$, $y_i \in R^m$, $i = 1, \ldots, N$. Such samples are transferred through another layer unlike the input layer, in which they can be enhanced as in the following equation:

$$O_j\left(\alpha_j x_i + \beta_j\right) = \frac{1}{1 + e^{-(\alpha_j x_i + \beta_j)}}, \beta_j \in [0, S], \alpha_j \in [-S, S] \tag{1}$$

where α_j and β_j are weights between layers, input layer and improved one, and the bias respectively. In addition, S is the parameter tuning coefficient and is a scale factor. The RVFL output layer after that can have an output obtained through the weight w as follows

$$Z = Fw, w \in R^{n+P}, F = [F_1, F_2] \tag{2}$$

where F represents the samples of the input data matrix that contains F_1 and F_2 represents the output of the improving layer.

$$F_1 = \begin{bmatrix} x_{11} & \ldots & x_{1n} \\ \vdots & \ddots & \vdots \\ x_{N1} & \ldots & x_{Nn} \end{bmatrix},$$
$$F_2 = \begin{bmatrix} G_1(\alpha_1 x_1 + \beta_1) & \ldots & G_P(\alpha_P x_1 + \beta_P) \\ \vdots & \ddots & \vdots \\ G_1(\alpha_1 x_N + \beta_1) & \ldots & G_P(\alpha_P x_N + \beta_P) \end{bmatrix} \tag{3}$$

The output weight **w** is updated by the ridge regression [45] or by the Moore-Penrose pseudo-inverse [45], [46].

$$w = \left(F^T F + \frac{I}{C}\right)^{-1} F^T Z \tag{4}$$
$$w = F^{\dagger} Z(5) \tag{5}$$

where I, $\dagger$ and C are, the identity matrix, the Moore-Penrose pseudo-inverse and a coefficient of the trading-off, respectively.

B. HENRY GAS SOLUBILITY OPTIMIZATION

In this section, we introduce the steps of the HGSO which simulates the physical behavior defined by Henr's law.

The HGSO, like other Physics-based algorithms, starts by constructing a set of N positions for the gases (X) and this process is formulated as

$$X_i = Lb + rand * (\text{Ub-Lb}), rand \in [0, 1] \tag{6}$$

where Lb and Ub are the lower and upper values in the search space, respectively.

The second step is to cluster the solutions in equal groups equivalent to the number of gas types and each group has the same number of gases. In addition, each of them has the same Henry's constant that defined as

$$H_j = l \times r_1, \quad j = 1, 2, \ldots, N_g$$

where r_1 is a random number and l is a constant value set to 5E-2, while N_g represents the number of groups. The next step is to assess the gas in each group to determine the best gas in each group. Followed by determining the best gas overall

the groups. Thereafter, the Henr's coefficient for the j-th group will be updated using the following equation

$$H_j(t+1) = H_j(t) \times \exp\left(-C_j \times \left(\frac{1}{T(t)} - \frac{1}{T^{\theta}}\right)\right), \quad T(t) = \exp\left(-\frac{t}{iter}\right) \tag{7}$$

where T, T^{θ}, and $iter$ are the temperature, constant value (set to 298.15), and the maximum number of iterations.

The next step in HGSO is to update the solubility of each solution among all groups (S_{ij}) using the following equation.

$$S_{ij}(t) = K \times H_j(t+1) \times P_{ij}(t) \tag{8}$$

where K is a constant and $P_{ij}(t)$ represents the partial pressure on i-th gas on j-th cluster j and its defined as

$$P_{ij}(t) = l_2 \times r_1, \quad j = 1, 2, \ldots, N_g, \quad l_2 = 100$$

The HGSO go to update the position of the i-th gas in the j-th group using the following equation:

$$X_{ij}(t+1) = X_{ij}(t) + F \times r \times \eta \times \left(X_{ib}(t) - X_{ij}(t)\right) + F \times r \times \alpha \times \left(S_{ij}(t) \times X_{ib}(t) - X_{ij}(t)\right) \tag{9}$$

$$\text{Where } \eta = \beta \times exp(-\frac{F_b(t) + \epsilon}{F_{ij}(t) + \epsilon}) \tag{10}$$

In Equation (10), the F_{ij} is the fitness value of the solution i on the group j and F_b is the best fitness value. F is a flag to change the direction gas. η represents the ability of the i-th gas in the group j to interact with other gases in the same group. Whereas, the $\alpha = 1$ represents the influence of other gases on the i-th gas in the j-th group. The HGSO use the following equation to escape the local point which determine the worst N_w solutions.

$$N_w = N \times r \times (c_2 - c_1) + c_1, \quad c_1 = 0.1, \ and \quad c_2 = 0.2 \tag{11}$$

Then those solutions are updated using the following equation

$$G_{ij} = G_{ij}^{min} + r \times \left(G_{ij}^{max} - G_{ij}^{min}\right) \tag{12}$$

G_{ij} is the solution i in the group j which belongs to the worst solutions.

C. THE PROPOSED HGSO-RVFL METHOD

The proposed model for predicting UTS of FSW is based on improving RVFL performance using a new swarm algorithm called HGSO. The proposed HGSO-RVFL contains two phases, in the first phase, the training phase, the initial values for the parameters of HGSO, and RVFL are received as well as the training set, then the initial values for N solutions (X) are generated which represent the parameters of the RVFL. Each one of these solutions refers to an RVFL configuration and to evaluate the quality of this configuration, it is learned using the training set and the performance of its output is computed using the root mean square error. After, computing the fitness value for all configurations (solutions), the best configuration is determined which has the smallest fitness value. The next step is to compute updating other configurations using HGSO operators. This process is performed until the stop conditions are satisfied and return by the best configuration. Then, the testing set is applied to this best configuration to assess its performance. Details of these two phases are given in the following sections.

1) TRAINING PHASE

This phase starts by receiving the input set and dividing it into training (70%) and testing set (30%). Then, the initial value for the parameters of the proposed HGSO-RVFL model such as number of solutions (N), dimension of each solution N_{par} (number of parameters), number of iterations are set. Thereafter, construct the initial solutions X using the following equation

$$x_{ij} = l_j + r \times \left(u_j - l_j\right), \quad i = 1, \ldots, N, \quad j = 1, \ldots, N_{par} \tag{13}$$

where u_j and l_j are the upper and lower boundaries at j th parameter, respectively. $r \in [0, 1]$ random value. For clarity, assume the i-th solution $x_i = [x_{i1}, x_{i2}, x_{i3}, x_{i4}, x_{i5}, x_{i6}, x_{i7}] = [N_h, Bias, link, AF, RT, mode, Scale_m]$. $x_{i1} \in [1, 2000]$ represents the number of hidden neuron; the value of $x_{i2} \in \{0, 1\}$ indicates either there is a bias in the output layer or not. The value of $x_{i3} \in \{0, 1\}$ is used if there is a direct link to output layer or not; while, the value of $x_{i4} \in \{1, 2, 3, 4, 5\}$ represents the type of the objective function (i.e., sig, tribas, radbas, hardlim, sin, and sign). The $x_{i5} \in \{1, 2\}$ is used to determine the kind of the randomization approach that applied to set the value of the weights (Uniform, and Gaussian);$x_{i6} \in \{1, 2\}$ is the approach used to improve the weights (Moore-Penrose pseudoinverse, and regularized least square). The value of $x_{i7} \in \{1, 2, 3\}$ is applied to determine the type of scaling the features here; and there are three types a) all neurons, b) each hidden neuron separately, and c) the randomization range of the uniform distribution. For example, $x_i = [200, 1, 1, 3, 1, 2, 2]$ indicates that the current configuration of RVFL contains 200 neurons with bias and direct link. In addition, radbas is used as an activation function, while weights are generated according to a uniform distribution. The regularized least square is sued to update weights with scale the features for each hidden neuron separately.

To assess the quality of each configuration, the training set is passed through the neurons and the final output (Y_P) is computed then the quality of this output is computed by using the following equatio

$$Fit_i = \sqrt{\frac{\sum_{i=1}^{Ns} (Y_P - Y_T)^2}{Ns}} \tag{14}$$

where Y_T is the original output, and Ns represents the number of samples in the training set. Thereafter, the best configuration (X_b) is determined and according to its value, the other

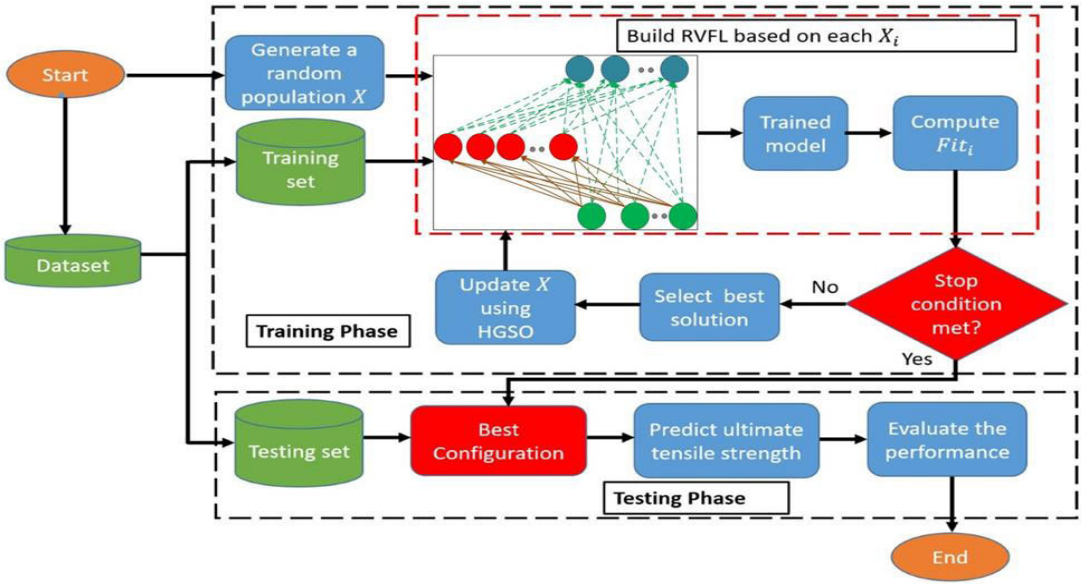

FIGURE 2. The HGSO-RVFL technique for predicting UTS.

configurations will be updated, in addition to using the operators of the HGSO as discussed in section B. Then the terminal conditions are checked; if they are met, then return by the best configuration otherwise, repeat the previous steps again.

2) TESTING PHASE

In this phase, the testing set is applied to assess the performance of the best configuration X_b by passing its samples to the input neurons and computing the final output. Then evaluate the output quality by computing the RMSE as defined in Equation (14). The HGSO-RVFL framework is shown in Fig.2.

TABLE 1. Chemical compositions of AA6061-T6 alloy (wt. %).

Components	Al	Mn	Si	Fe	Zn	Ti	Cr	Mg	Cu
wt.%	Bal.	0.03	0.61	0.20	0.02	0.01	0.13	0.81	0.29

III. MATERIALS AND METHOD

In order to collect data to construct the HGSO-RVFL model, experimental information of literature [47] has been used as well as the regression model given in Eq. 15 for UTS. Two 5 mm thickness AA6061-T6 aluminum alloys plates have been used to produce FSWD butt joints as shown in Fig. 3. The chemical composition of AA6061- T6 is shown in Table 1. UTS of AA6061-T6 aluminum alloys is 312 MPa. Five tools with different pin geometries made of molybdenum-based high-speed steel were used to produce the FSWD joints: simple square (SS), simple cylindrical (SC), simple tapered (ST), cylindrical with threads (CT), and tapered with threads (TT) as shown in Fig. 4. All tools had the same dimension of shoulder diameter of 18 mm with a concave of 6°, pin diameter of 6 mm and pin length of 4.7 mm.

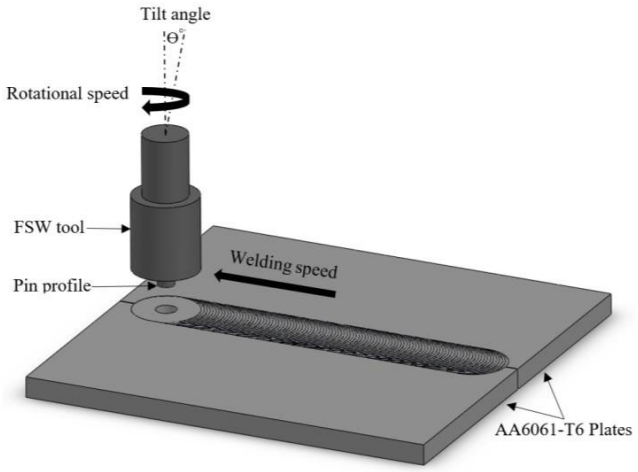

FIGURE 3. Schematic diagram of FSW and process parameters.

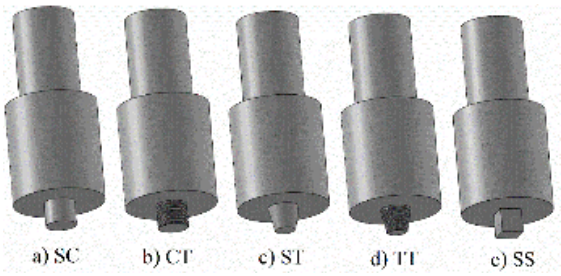

FIGURE 4. Different tool Pin profiles used in FSW process; (a) simple cylindrical, (b) cylindrical with threads, (c) simple tapered, (d) tapered with threads, and (e) simple square.

The base of the pin and the tip diameter of TT and ST were 4 and 6 mm, respectively, while the plunge depth was 0.1 mm. FSW parameters used in the proposed model and working

TABLE 2. FSW parameters and working range [47].

Parameters	Levels				
	-2	-1	0	+1	+2
Pin profile, P	SS	TT	SC	CT	ST
Rotational speed, N (rpm)	850	1000	1150	1300	1450
Welding speed, S (mm/min)	30	50	70	90	110
Tilt angle, T	1 °	2 °	3 °	4 °	5 °

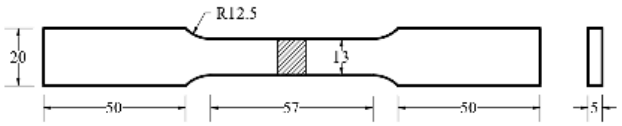

FIGURE 5. Dimensions of tensile sample (ASTM E8M-04).

range are shown in Table 2. Tensile samples were prepared based on ASTM E8M-04 standard dimensions as described in Fig. 5. Each experiment had three replicates and the mean was computed for each experimental set. Table 3 shows the FSW parameters for the welded AA6061-T6 plates and the measured UTS used to create the HGSO-RVFL model.

$$\begin{aligned} UTS = {} & 276.62 + 14.96\,(P) - 1.18\,(N) - 7.32\,(S) + 0.21T \\ & +3.79\,(P)\,(N) + 8.07\,(P)\,(S) + 0.46\,(P)\,(T) \\ & +9.35\,(N)\,(S) + 0.32\,(N)\,(T) + 3.42\,(S)\,(T) \\ & -30.86\left(P^2\right) - 3.40\left(N^2\right) - 3.01\left(S^2\right) - 4.59\left(T^2\right) \end{aligned} \tag{15}$$

IV. RESULTS AND DISCUSSION

A. COMPARISON OF EXPERIMENTAL RESULTS WITH PREDICTED RESULTS OF HGSO-RVFL, ANFIS, AND KNN MODELS FOR UTS

In this study, we proposed HGSO-RVFL as the main algorithm. However, we added two other algorithms to compare their results with the result of HGSO-RVFL and demonstrate the accuracy of the proposed model. The measured UTS results are compared with the predicted results by RVF–HGOS model as shown in Fig. 6. The HGSO-RVFL model showed a high correlation with experimental results due to its high prediction rate. To confirm the strength of the HGSO-RVFL model in the prediction process, ANFIS and K Nearest Neighbor algorithm (KNN) models have been constructed with the same input data and then compared with the experimental data. The ANFIS model displayed less predictability than HGSO-RVFL model as shown in Fig.7, while KNN model had the lowest degree of predictability as shown in Fig.8. This indicates that the KNN suffers from overfitting and needs more experiments as training set. Therefore, the correlation between HGSO-RVFL predicted data and the corresponding experimental data is better than those obtained by ANFIS or KNN thanks to the integration between advanced ANN technique (RVFL) and robust metaheuristic technique (HGSO) that successfully predicts the UTS of FSW process. Since the HGSO aims to find the optimal configuration that provides RVFL with a suitable tool to avoid the limitations in traditional ANFIS and KNN such as absence of direct link between input and output which leads to overfitting.

In addition, the percentage error E_i and the average percentage error E_{av} have been used to assess the performance of HGSO-RVFL algorithm. The E_i and E_{av} are defined

TABLE 3. Design matrix used to train HGSO-RVFL model [47].

Test No	Welding Parameters				Measured UTS (MPa)
	N (rpm)	S (mm/min)	T	P	
1	1000	50	2°	TT	249.38
2	1300	50	2°	TT	211.26
3	1000	90	2°	TT	180.41
4	1000	50	4°	TT	244.49
5	1000	50	2°	CT	258.37
6	1300	90	4°	CT	261.5
7	1000	90	4°	CT	252.07
8	1300	50	4°	CT	253.44
9	1300	90	2°	CT	255.93
10	1300	90	4°	TT	209.59
11	1000	50	4°	CT	250.46
12	1000	90	2°	CT	255.44
13	1000	90	4°	TT	183.81
14	1300	50	2°	CT	254.28
15	1300	50	4°	TT	187.38
16	1300	90	2°	TT	198.06
17	1450	70	3°	SC	272.99
18	850	70	3°	SC	265.62
19	1150	110	3°	SC	255
20	1150	30	3°	SC	286.72
21	1150	70	5°	SC	270.88
22	1150	70	1°	SC	258.18
23	1150	70	3°	ST	154.95
24	1150	70	3°	SS	164
25	1150	70	3°	SC	288.1
26	1150	70	3°	SC	286.02
27	1150	70	3°	SC	264.65
28	1150	70	3°	SC	283.92
29	1150	70	3°	SC	253.04
30	1150	70	3°	SC	283.99

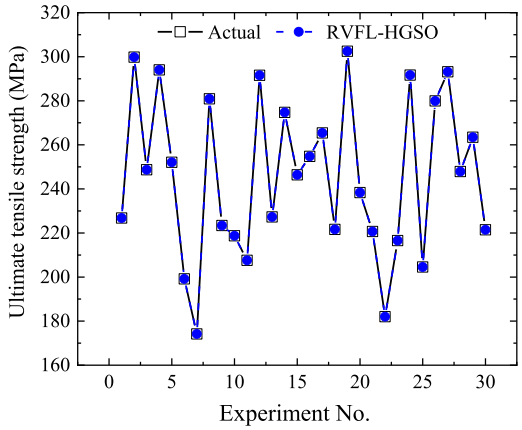

FIGURE 6. UTS results of experimental values versus HGSO-RVFL modified values.

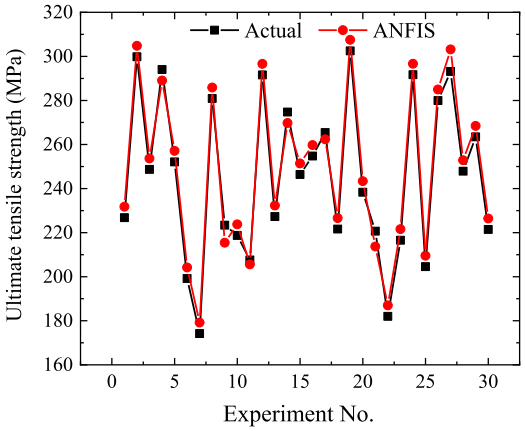

FIGURE 7. UTS results of experimental values versus ANFIS values.

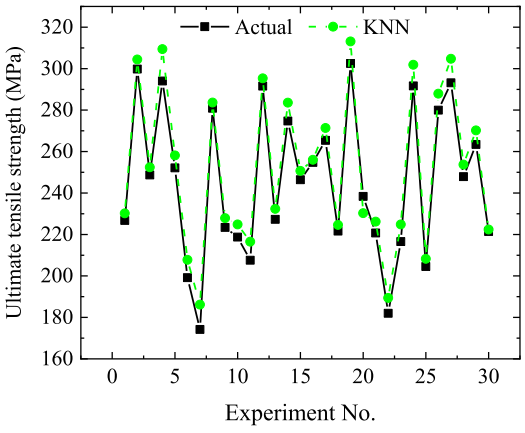

FIGURE 8. UTS results of experimental values versus KNN values.

in equations. (16) and (17) respectively.

$$E_i = \left| \frac{UTS_i - UTS_i^P}{UTS_i} \right| \times 100 \tag{16}$$

$$E_{av} = \frac{1}{n} \sum_{i=1}^{n} E_i \tag{17}$$

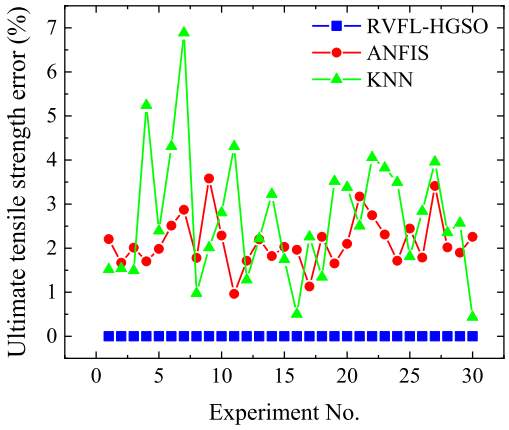

FIGURE 9. HGSO-RVFL error versus ANFIS and KNN.

where, i is the experiment number, E_i is the percentage error; $UTS_i$and UTS_i^P are the experimental and predicted UTS, respectively. E_{av} denotes the average value of the percentage error. Fig. 9 demonstrate the prediction error for HGSO-RVFL, ANFIS, and KNN models which are 0 %, 2.139 %, and 2.693 %, respectively. This indicates that ANFIS and KNN models suffer from overfitting. Therefore, HGSO-RVFL model can be used to predict UTS values better than other investigated models. From the abovementioned discussion, the HGSO-RVFL is proved to be a reliable and strong algorithm to predict mechanical properties of FSWD.

B. CHECKING VALIDATION OF THE MODEL

Figure 10 (a), (b) and (c) demonstrate the validity of HGSO-RVFL, ANFIS, and KNN models to predict UTS. The predicted values are scattered around the line for all three models. For the HGSO-RVFL model, plotted values are regularly distributed around the line as shown in Fig. 10 (a), which indicates the accuracy and fitness of the model because of the ability of HGSO algorithm to discover the optimal configuration that provides RVFL a suitable tool for avoiding constraints in conventional ANFIS and KNN such as there is no direct link between inputs and outputs leading to over-fitting, while values are less uniformly distributed around the line for ANFIS model as shown in Fig. 10 (b), they are also randomly distributed around the line for KNN model as shown in Fig. 10 (c) which indicates the worst fitness among all investigated models. The above discussion illustrates an excellent prediction capability of the HGSO-RVFL model.

C. STATISTICS FOR HGSO-RVFL MODEL COMPARED WITH ANFIS, AND KNN MODELS

The obtained results by different models are checked using different statistical criteria such as the root mean square error (RMSE), the mean absolute error (MAE), the coefficient of determination (R2), the mean relative estimate error (MRE), and the coefficient of variance (COV). The values of these statistical coefficients are tabulated in Table 4. R2 equals 1, 1, and 0.9997 for the HGSO-RVFL, ANFIS, and KNN models

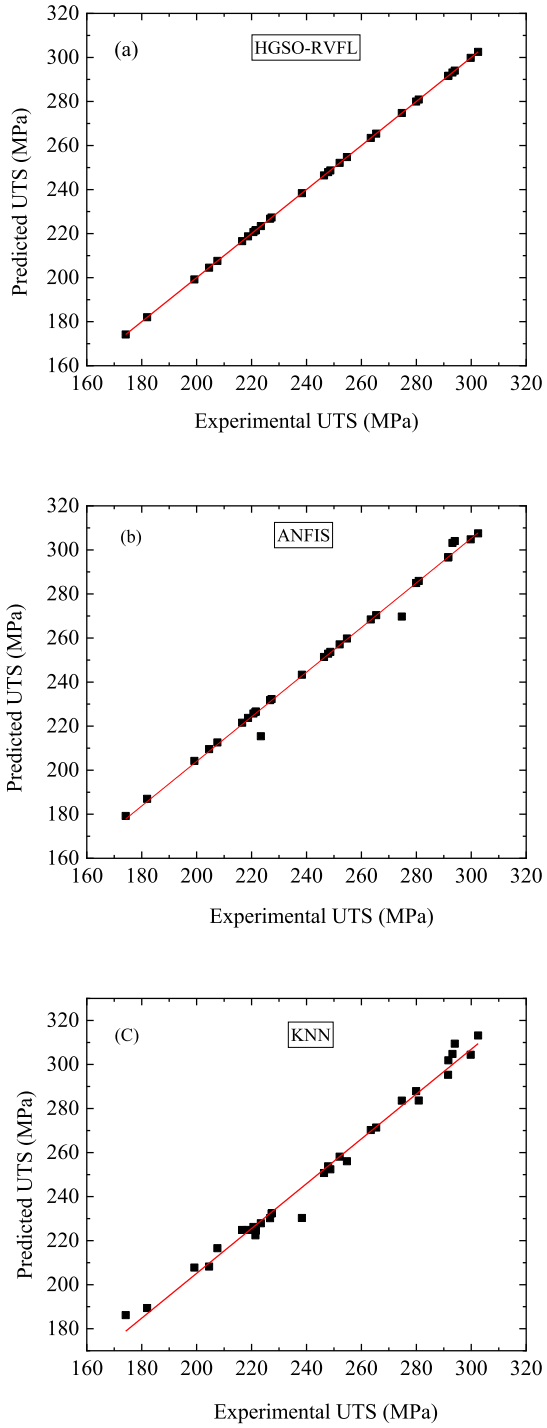

FIGURE 10. Fitting of UTS data (a) HGSO-RVFL model, (b) ANFIS model and (c) KNN model.

respectively, which indicates a high correlation between the experimental and the predicted data of HGSO-RVFL compared with the other two models. Moreover, the RMSE of HGSO-RVFL model (3.0482E-12) is lower than the ANFIS model (4.1267E-06) and KNN model (4.2295). MAE, MRE, and COV values of HGSO-RVFL model are lower than that of the other two models, thus the prediction of HGSO-RVFL technique has much adequacy to predict the UTS of FSWD joints with high accuracy.

TABLE 4. Statistical results of the developed models.

Statistics	HGSO-RVFL	ANFIS	KNN
R2	1	1	0.9997
RMSE	3.0482E-12	4.1267E-06	4.2295
MRE	1.1642E-14	6.7562E-09	0.0002
MAE	2.9535E-12	3.3530E-06	3.0996
COV	1.1683E-12	1.5816E-06	1.6215

D. PREDICTION OF FSW PROCESS PARAMETERS

The developed HGSO-RVFL model was applied to study and predict the parameters of FSW process as shown in Fig.11 (a-c) where a significant agreement was observed between the predicted results and the experimental results, indicating the high ability of the developed model to predict the ideal welding parameters that achieve the optimal UTS.

Fig. 11a illustrates the effects of rotational speed and welding speed on UTS. It was observed that base material UTS (312 MPa) is higher than the UTS for all investigated joints regardless of rotational speed and welding speed used in the FSW process. Increasing the rotational speed and decreasing the welding speed increases the tensile stress to reach the maximum value (288.1 MPa) at (1150 rpm - 70 mm / min), and (286.72 MPa) at (1150 rpm - 30 mm / min), then gradually decreases with increasing welding speed due to the increase in heat input to the welding region. Increasing the rotational speed of the welding tool increases the heat input and affects the uniform flow behavior of the material. At the same time, the lower rotational speed produces less heat input, which results in the lack of stirring action. Therefore, excessive grain growth, solubilization and reprecipitating lead to a decrease in UTS of AA6061 FS welded aluminum alloys. Fig. 11b shows the effect of rotational speed and tool pin profile where simple cylindrical pin profile produces maximum UTS at 1450 rpm whereas tensile stress gradually decreases at a rotation speed of 1150 rpm using a tapered pin with threading, cylindrical pin with threading, and simple tapered screw, respectively to reach minimum value using simple square pin profile. Fig. 11c shows the effects of rotational speed and tool tilt angle. UTS increases with increasing tilt angle and rotational speed to reach peak value at 3° and 1450 rpm then decreases with increasing these parameters more than these values. Increasing the tilt angle causes poor bonding due to excessive reduction of frictional heat generation which increases average grain size while decreasing tilt angle leads to poor bonding because of high frictional heat generation [48]. Fig. 11d plots the effect of tool pin profile and welding speed on the UTS of the FSWD joints. The plot shows that simple cylindrical pin profile gives the maximum UTS at 30 mm/min, while a gradual decrease of tensile stress is observed at welding speed of 70 mm/min using tapered pin

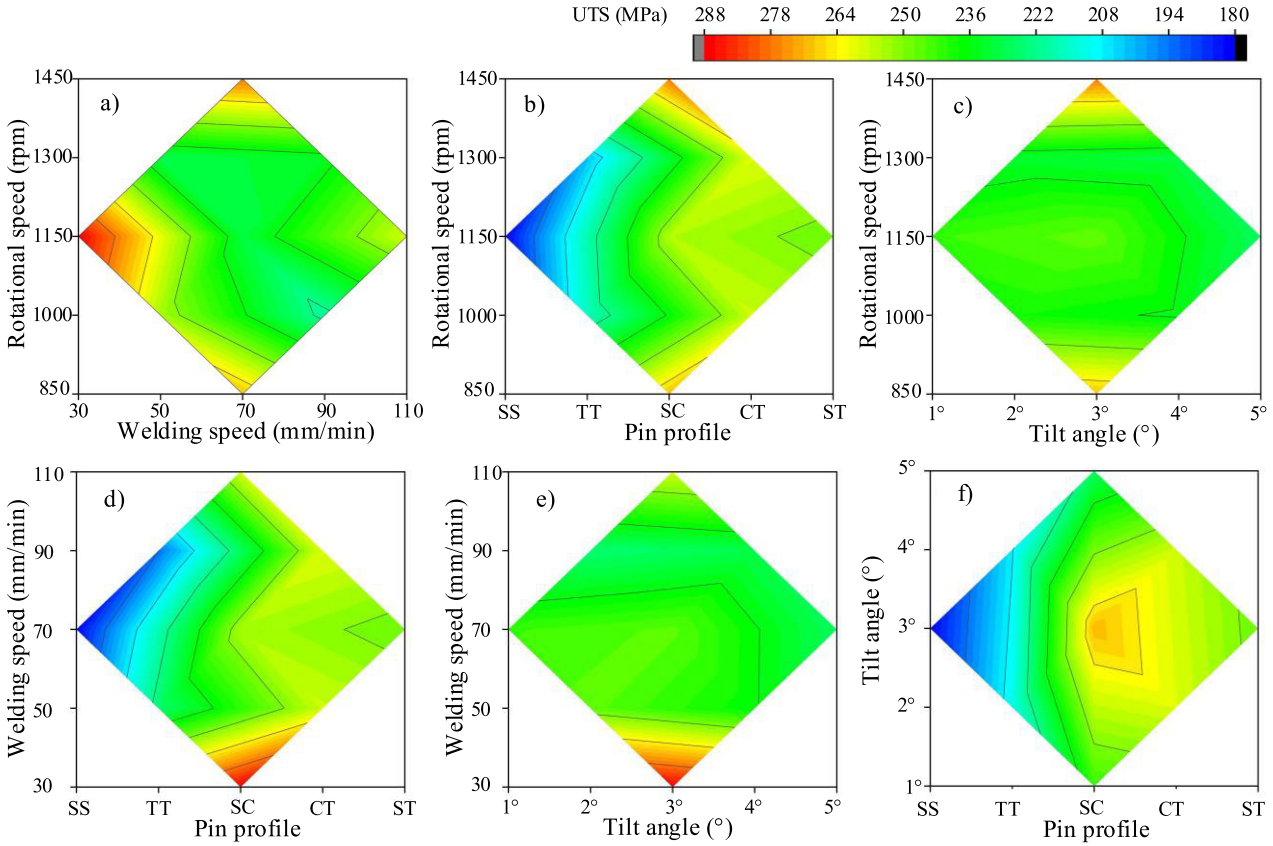

FIGURE 11. Contour plots showing the effect of (a) Rotation speed – Welding speed, (b) Rotation speed – Pin profile, (c) Rotation speed – Tilt angle, (d) Welding speed – Pin profile, (e) Welding speed – Tilt angle, and (f) Tilt angle – Pin profile on UTS for the developed HGSO-RVFL model.

with threads, cylindrical pin with threads, and simple tapered pin profile respectively to reach minimum value using simple square pin profile. Finer grain size is achieved for taper tools compared to other tools as a result of better flow of plasticized material, thereby producing a sound joint [49].

The effects of welding speed and tool tilt angle on UTS are shown in Fig. 11e. As welding speed increases, UTS decreases. Increasing in tilt angle results in increasing the UTS to reach the maximum value at 3° and 30 mm/min, and then gradually decreases as these two parameters increase. Increasing the tilt angle of the welding tool leads to an increase in the vertical force and torque, this may lead to an increase in the contact between the tool and the workpiece and then the highest heat inputs are achieved which causes a thermal softening of the deformed material and an increase in the flow of downward materials, where the restoration of grains are obtained in stir zone that occurs in conjunction with the deformation, and this process is called dynamic recrystallization, which leads to the grain refinement during welding [50]. Fig. 11f shows the effect of tool tilt angle and tool pin profile. Maximum UTS value is achieved by simple cylindrical tool pin profile and tilt angle of 3° while this value gradually decreases at the same tilt angle for cylindrical pin with threads and simple tapered pin profile, respectively until it reaches the minimum value using simple square pin profile.

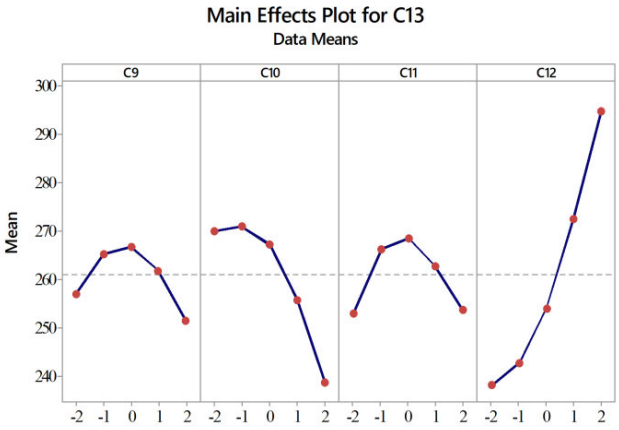

FIGURE 12. Main effect plot of FSW parameters on the process response (UTS).

E. MAIN EFFECTS OF FSW WELDING PARAMETERS ON UTS

The main effect plot of different FSW parameters on the process response (UTS) is shown in Fig.12. In order to realize the maximum UTS, it is recommended to use a rotation speed of 1450 rpm or 1150 rpm and avoid using a rotation speed of 1300 rpm as it leads to minimal UTS. It is also

recommended to use a welding speed of 30 mm/min to obtain maximum UTS. It can also be noted that the use of a simple cylindrical pin profile or a cylindrical tapered pin profile can attain maximum UTS while simple square pin profile leads to impair UTS. A tilt angle of 3° can achieve maximal UTS while 5° leads to minimal UTS. Generally, the HGSO-RVFL model can successfully confirm that the use of a simple cylindrical tool, a tilt angle of 3°, a rotation speed of 1150 rpm, and a welding speed of 30 mm/min can achieve a high quality AA6061-T6 aluminum alloy welding joint.

V. CONCLUSION

In this paper, we proposed a novel ANN model to predict UTS of the FSWD joints of aluminum alloy AA6061-T6 as functions of welding speed, rotational speed, tilt angle, and tool pin profile. HGSO algorithm was used to optimize the performance of RVFL network, the validity of the model was checked, and the effect of the process parameters on the mechanical properties of the joint was discussed. The following conclusions can be drawn:

- HGSO technique can successfully find the optimal configuration that provides RVFL with a suitable tool to avoid the limitations in traditional algorithms such as absence of direct link between input and output which leads to overfitting.
- The developed HGSO-RVFL model can be used to predict the responses of experimental values at R2 of 1.
- The HGSO-RVFL model can successfully confirm that using simple cylindrical tool, 3° tilt angle, rotation speed 1150 rpm, and welding speed 30mm / min can achieve high quality aluminum alloy AA6061-T6 FSWD joint.
- The HGSO-RVFL model has high predictability of FSW parameters to reach the optimum mechanical properties and is recommended for other engineering applications.

ACKNOWLEDGMENT

The authors would like to acknowledge the academic and technical support from Laboratory of Materials Processing and Die & Mould Technology at Huazhong University of Science and Technology.

REFERENCES

[1] D. A. Kumar, P. Biswas, S. Tikader, M. M. Mahapatra, and N. R. Mandal, "A study on friction stir welding of 12 mm thick aluminum alloy plates," *J. Mar. Sci. Appl.*, vol. 12, no. 4, pp. 493–499, Dec. 2013.

[2] K. A. Matori, M. Tamjidy, F. Fadaeifard, F. Gharvi, H. T. Baherodin, and S. Paslar, "Optimization parameters of friction stir lap welding of aluminum alloy AA6061-T6," *J. Appl. Sci.*, vol. 15, no. 3, pp. 465–473, Mar. 2015.

[3] C. G. Rhodes, M. W. Mahoney, W. H. Bingel, R. A. Spurling, and C. C. Bampton, "Effects of friction stir welding on microstructure of 7075 aluminum," *Scripta Mater.*, vol. 36, no. 1, pp. 69–75, Jan. 1997.

[4] W. W. Thomas, "International patent application No. PCT/GB92," Patent Appl. GB 9 125 978.8, Jun. 1991.

[5] R. S. Mishra and Z. Y. Ma, "Friction stir welding and processing," *Mater. Sci. Eng. Rep.*, vol. 50, nos. 1–2, pp. 1–78, 2005.

[6] O. S. Salih, H. Ou, W. Sun, and D. G. McCartney, "A review of friction stir welding of aluminium matrix composites," *Mater. Des.*, vol. 86, pp. 61–71, Dec. 2015.

[7] L. E. Murr, "A review of FSW research on dissimilar metal and alloy systems," *J. Mater. Eng. Perform.*, vol. 19, no. 8, pp. 1071–1089, Nov. 2010.

[8] G. K. Padhy, C. S. Wu, and S. Gao, "Friction stir based welding and processing technologies–processes, parameters, microstructures and applications: A review," *J. Mater. Sci. Technol.*, vol. 34, no. 1, pp. 1–38, Jan. 2018.

[9] C. Rajendran, K. Srinivasan, V. Balasubramanian, H. Balaji, and P. Selvaraj, "Effect of tool tilt angle on strength and microstructural characteristics of friction stir welded lap joints of AA2014-T6 aluminum alloy," *Trans. Nonferrous Met. Soc. China*, vol. 29, no. 9, pp. 1824–1835, Sep. 2019.

[10] R. Palanivel, P. Koshy Mathews, N. Murugan, and I. Dinaharan, "Effect of tool rotational speed and pin profile on microstructure and tensile strength of dissimilar friction stir welded AA5083-H111 and AA6351-T6 aluminum alloys," *Mater. Des.*, vol. 40, pp. 7–16, Sep. 2012.

[11] M. I. Costa, D. Verdera, C. Leitão, and D. M. Rodrigues, "Dissimilar friction stir lap welding of AA 5754-H22/AA 6082-T6 aluminium alloys: Influence of material properties and tool geometry on weld strength," *Mater. Des.*, vol. 87, pp. 721–731, Dec. 2015.

[12] W. F. Xu, X. K. Wu, J. Ma, H. J. Lu, and Y. X. Luo, "Abnormal fracture of 7085 high strength aluminum alloy thick plate joint via friction stir welding," *J. Mater. Res. Technol.*, vol. 8, no. 6, pp. 6029–6040, Nov. 2019.

[13] S. Rajakumar, C. Muralidharan, and V. Balasubramanian, "Influence of friction stir welding process and tool parameters on strength properties of AA7075-T6 aluminium alloy joints," *Mater. Des.*, vol. 32, no. 2, pp. 535–549, Feb. 2011.

[14] A. H. Elsheikh, S. W. Sharshir, M. Abd Elaziz, A. E. Kabeel, W. Guilan, and Z. Haiou, "Modeling of solar energy systems using artificial neural network: A comprehensive review," *Sol. Energy*, vol. 180, pp. 622–639, Mar. 2019.

[15] H. A. Babikir, M. A. Elaziz, A. H. Elsheikh, E. A. Showaib, M. Elhadary, D. Wu, and Y. Liu, "Noise prediction of axial piston pump based on different valve materials using a modified artificial neural network model," *Alexandria Eng. J.*, vol. 58, no. 3, pp. 1077–1087, Sep. 2019.

[16] K. Singh, S. K. Rajput, and Y. Mehta, "Modeling of the hot deformation behavior of a high phosphorus steel using artificial neural networks," *Mater. Discovery*, vol. 6, pp. 1–8, Oct. 2016.

[17] M. C. Dixit, N. Srivastava, and S. K. Rajput, "Modeling of flow stress of AA6061 under hot compression using artificial neural network," *Mater. Today, Proc.*, vol. 4, no. 2, pp. 1964–1971, 2017.

[18] T. F. Flint, J. A. Francis, and M. C. Smith, "A semi-analytical solution for the transient temperature field generated by a volumetric heat source developed for the simulation of friction stir welding," *Int. J. Thermal Sci.*, vol. 138, pp. 586–595, Apr. 2019.

[19] K. H. Salman, A. H. Elsheikh, M. Ashham, M. K. A. Ali, M. Rashad, and Z. Haiou, "Effect of cutting parameters on surface residual stresses in dry turning of AISI 1035 alloy," *J. Brazilian Soc. Mech. Sci. Eng.*, vol. 41, no. 8, p. 349, Aug. 2019.

[20] A. R. Shahani and A. Farrahi, "Experimental investigation and numerical modeling of the fatigue crack growth in friction stir spot welding of lap-shear specimen," *Int. J. Fatigue*, vol. 125, pp. 520–529, Aug. 2019.

[21] A. H. Elsheikh, J. Guo, Y. Huang, J. Ji, and K.-M. Lee, "Temperature field sensing of a thin-wall component during machining: Numerical and experimental investigations," *Int. J. Heat Mass Transf.*, vol. 126, pp. 935–945, Nov. 2018.

[22] A. H. Elsheikh, S. W. Sharshir, A. S. Ismail, R. Sathyamurthy, T. Abdelhamid, E. M. A. Edreis, A. E. Kabeel, and Z. Haiou, "An artificial neural network based approach for prediction the thermal conductivity of nanofluids," *Social Netw. Appl. Sci.*, vol. 2, no. 2, p. 235, Feb. 2020.

[23] K. Andersen, G. E. Cook, G. Karsai, and K. Ramaswamy, "Artificial neural networks applied to arc welding process modeling and control," *IEEE Trans. Ind. Appl.*, vol. 26, no. 5, pp. 824–830, Sep./Oct. 1990.

[24] D. S. Nagesh and G. L. Datta, "Prediction of weld bead geometry and penetration in shielded metal-arc welding using artificial neural networks," *J. Mater. Process. Technol.*, vol. 123, no. 2, pp. 303–312, Apr. 2002.

[25] D. S. Nagesh and G. L. Datta, "Genetic algorithm for optimization of welding variables for height to width ratio and application of ANN for prediction of bead geometry for TIG welding process," *Appl. Soft Comput.*, vol. 10, no. 3, pp. 897–907, Jun. 2010.

[26] S. Pal, S. K. Pal, and A. K. Samantaray, "Artificial neural network modeling of weld joint strength prediction of a pulsed metal inert gas welding process using arc signals," *J. Mater. Process. Technol.*, vol. 202, nos. 1–3, pp. 464–474, Jun. 2008.

[27] R. Palanivel, I. Dinaharan, and R. F. Laubscher, "Application of an artificial neural network model to predict the ultimate tensile strength of friction-welded titanium tubes," *J. Brazilian Soc. Mech. Sci. Eng.*, vol. 41, no. 2, p. 111, Feb. 2019.
[28] V. M. Dehabadi, S. Ghorbanpour, and G. Azimi, "Application of artificial neural network to predict Vickers microhardness of AA6061 friction stir welded sheets," *J. Central South Univ.*, vol. 23, no. 9, pp. 2146–2155, 2016.
[29] H. Okuyucu, A. Kurt, and E. Arcaklioglu, "Artificial neural network application to the friction stir welding of aluminum plates," *Mater. Des.*, vol. 28, no. 1, pp. 78–84, Jan. 2007.
[30] D. Oliva, M. A. Elaziz, A. H. Elsheikh, and A. A. Ewees, "A review on meta-heuristics methods for estimating parameters of solar cells," *J. Power Source*, vol. 435, Sep. 2019, Art. no. 126683.
[31] A. H. Elsheikh and M. Abd Elaziz, "Review on applications of particle swarm optimization in solar energy systems," *Int. J. Environ. Sci. Technol.*, vol. 16, no. 2, pp. 1159–1170, Feb. 2019.
[32] M. A. Elaziz, A. H. Elsheikh, and S. W. Sharshir, "Improved prediction of oscillatory heat transfer coefficient for a thermoacoustic heat exchanger using modified adaptive neuro-fuzzy inference system," *Int. J. Refrig.*, vol. 102, pp. 47–54, Jun. 2019.
[33] T. A. Shehabeldeen, M. A. Elaziz, A. H. Elsheikh, and J. Zhou, "Modeling of friction stir welding process using adaptive neuro-fuzzy inference system integrated with harris hawks optimizer," *J. Mater. Res. Technol.*, vol. 8, no. 6, pp. 5882–5892, Nov. 2019.
[34] S. E. De Leon-Aldaco, H. Calleja, and J. Aguayo Alquicira, "Metaheuristic optimization methods applied to power converters: A review," *IEEE Trans. Power Electron.*, vol. 30, no. 12, pp. 6791–6803, Dec. 2015.
[35] F. A. Essa, M. A. Elaziz, and A. H. Elsheikh, "An enhanced productivity prediction model of active solar still using artificial neural network and harris hawks optimizer," *Appl. Thermal Eng.*, vol. 170, Apr. 2020, Art. no. 115020.
[36] I. N. Tansel, M. Demetgul, H. Okuyucu, and A. Yapici, "Optimizations of friction stir welding of aluminum alloy by using genetically optimized neural network," *Int. J. Adv. Manuf. Technol.*, vol. 48, nos. 1–4, pp. 95–101, Apr. 2010.
[37] M. Akbari, M. H. Shojaeefard, P. Asadi, and A. Khalkhali, "Hybrid multi-objective optimization of microstructural and mechanical properties of b 4 C/A356 composites fabricated by FSP using TOPSIS and modified NSGA-II," *Trans. Nonferrous Met. Soc. China*, vol. 27, no. 11, pp. 2317–2333, Nov. 2017.
[38] M. Akbari, P. Asadi, P. Zolghadr, and A. Khalkhali, "Multicriteria optimization of mechanical properties of aluminum composites reinforced with different reinforcing particles type," *Proc. Inst. Mech. Eng., Part E, J. Process Mech. Eng.*, vol. 232, no. 3, pp. 323–337, Jun. 2018.
[39] M. R. M. Aliha, M. Shahheidari, M. Bisadi, M. Akbari, and S. Hossain, "Mechanical and metallurgical properties of dissimilar AA6061-T6 and AA7277-T6 joint made by FSW technique," *Int. J. Adv. Manuf. Technol.*, vol. 86, nos. 9–12, pp. 2551–2565, Oct. 2016.
[40] M. H. Shojaeefard, R. A. Behnagh, M. Akbari, M. K. B. Givi, and F. Farhani, "Modelling and Pareto optimization of mechanical properties of friction stir welded AA7075/AA5083 butt joints using neural network and particle swarm algorithm," *Mater. Des.*, vol. 44, pp. 190–198, Feb. 2013.
[41] A. K. Lakshminarayanan and V. Balasubramanian, "Comparison of RSM with ANN in predicting tensile strength of friction stir welded AA7039 aluminium alloy joints," *Trans. Nonferrous Met. Soc. China*, vol. 19, no. 1, pp. 9–18, Feb. 2009.
[42] M. W. Dewan, D. J. Huggett, T. Warren Liao, M. A. Wahab, and A. M. Okeil, "Prediction of tensile strength of friction stir weld joints with adaptive neuro-fuzzy inference system (ANFIS) and neural network," *Mater. Des.*, vol. 92, pp. 288–299, Feb. 2016.
[43] F. A. Hashim, E. H. Houssein, M. S. Mabrouk, W. Al-Atabany, and S. Mirjalili, "Henry gas solubility optimization: A novel physics-based algorithm," *Future Gener. Comput. Syst.*, vol. 101, pp. 646–667, 2019.
[44] Y.-H. Pao, G.-H. Park, and D. J. Sobajic, "Learning and generalization characteristics of the random vector functional-link net," *Neurocomputing*, vol. 6, no. 2, pp. 163–180, Apr. 1994.
[45] L. Zhang and P. N. Suganthan, "A comprehensive evaluation of random vector functional link networks," *Inf. Sci.*, vols. 367–368, pp. 1094–1105, Nov. 2016.
[46] C. L. P. Chen, "A rapid supervised learning neural network for function interpolation and approximation," *IEEE Trans. Neural Netw.*, vol. 7, no. 5, pp. 1220–1230, Sep. 1996.
[47] W. Safeen, S. Hussain, A. Wasim, M. Jahanzaib, H. Aziz, and H. Abdalla, "Predicting the tensile strength, impact toughness, and hardness of friction stir-welded AA6061-T6 using response surface methodology," *Int. J. Adv. Manuf. Technol.*, vol. 87, nos. 5–8, pp. 1765–1781, Nov. 2016.
[48] S. Shanavas and J. E. R. Dhas, "Parametric optimization of friction stir welding parameters of marine grade aluminium alloy using response surface methodology," *Trans. Nonferrous Met. Soc. China*, vol. 27, no. 11, pp. 2334–2344, Nov. 2017.
[49] A. Banik, B. S. Roy, J. D. Barma, and S. C. Saha, "An experimental investigation of torque and force generation for varying tool tilt angles and their effects on microstructure and mechanical properties: Friction stir welding of AA 6061-T6," *J. Manuf. Processes*, vol. 31, pp. 395–404, Jan. 2018.
[50] S. Shamsudeen and J. E. R. Dhas, "Optimization of multiple performance characteristics of friction stir welded joint with grey relational analysis," *Mater. Res.*, vol. 21, no. 6, 2018, Art. no. e20171050.

TAHER A. SHEHABELDEEN was born in Kafr El Sheikh, Egypt, in 1988. He received the B.S. degree in mechanical engineering from Kafrelsheikh University, Kafr El Sheikh, in 2010, and the M.S. degree in mechanical engineering from Benha University, Benha, Egypt, in 2017. He is currently pursuing the Ph.D. degree with the School of Materials Science and Engineering, Huazhong University of Science and Technology, Wuhan, China. From 2010 to 2017, he was a Research Assistant with the Faculty of Engineering, Kafrelsheikh University. His research interests include the friction stir welding of similar and dissimilar alloys, numerical simulation, and optimization of manufacturing processes using soft computing techniques.

MOHAMED ABD ELAZIZ received the B.S. and M.S. degrees in computer science and the Ph.D. degree in mathematics and computer science from Zagazig University, Egypt, in 2008, 2011, and 2014, respectively. From 2008 to 2011, he was an Assistant Lecturer with the Department of Computer Science. Since 2014, he has been a Lecturer with the Mathematical Department, Zagazig University. He is the author of more than 50 articles. His research interests include machine learning, signal processing, image processing, and metaheuristic techniques.

AMMAR H. ELSHEIKH was born in Elmahalla Alkubra, Egypt, in 1985. He received the B.Sc. and M.Sc. degrees in mechanical engineering from Tanta University, Tanta, Egypt, and the Ph.D. degree from the Huazhong University of Science and Technology, Wuhan, China. He is currently working as an Assistant Professor with the Production Engineering and Mechanical Design Department, Tanta University. His research interests include renewable energy, manufacturing systems, and the applications of ANN techniques in engineering problems. He is the author of more than 30 articles. He has been awarded the Academic Excellence Award of the Huazhong University of Science and Technology for Outstanding International Students, in 2018.

OSAMA FAROUK HASSAN received the B.S. degree in computer science from Zagazig University, in 1995, and the M.S. and Ph.D. degrees in computer science from Suez Canal University, Ismailia, Egypt, in 2011 and 2014, respectively. From 1997 to 2011, he was a Computer Specialist with the Faculty of Computers and Information, Suez Canal University. From 2011 to 2015, he was a Lecturer with the Community College, Unaizah, Qassim University, Saudi Arabia. From 2015 to 2018, he was a Lecturer and the Vice Dean with the Faculty of Computer Science, Nahda University, Beni Suef, Egypt. Since 2018, he has been a Lecturer with the Mathematical Department, Faculty of Science, Damanhour University, Egypt. He is the author of more than five articles. His research interests include signal processing, image processing, and machine learning.

YAJUN YIN was born in Hubei, China, in 1985. He received the Ph.D. degree in materials processing engineering from the Huazhong University of Science and Technology, Wuhan, China. He is currently an Associate Professor, the Main Technical Developer of the Research Team of InteCAST Software Center, Huazhong University of Science and Technology. His main research interests include the numerical simulation of the casting process, 3D printing, and hot isostatic pressing. He has published more than 20 articles, got five patent and six software copyrights. He has got the youth program fund of the Natural Science Foundation of China, the First and the Second Class of the China Postdoctoral Fund, and some others from the cooperation company, especially from the aerospace and weapons industry. He also won the First Prize of the Cooperative Innovation Achievements, (No. 3), in 2015, the First Prize of the Science and Technology of China Machinery Industry, in 2017 (No. 2), and the second prize of the National Science and Technology Progress Award, in 2018 (No. 5).

XIAOYUAN JI was born in 1986. He received the Ph.D. degree from the Huazhong University of Science and Technology, in 2013. He is currently a Lecturer with the School of Materials Science and Engineering. He developed the InteCAST-ERP software. He has published more than 50 articles, won two provincial and ministerial level awards, five software copyrights, and one patent. His research interests include algorithms, deep learning, artificial intelligence, data mining, big data, information management, and ERP for foundry enterprises.

XU SHEN received the M.S. and Ph.D. degrees from the Huazhong University of Science and Technology, in 2008 and 2016, respectively. He is currently a Lecturer with the School of Materials Science and Engineering. His research interests include numerical simulation, titanium alloys, solidification, modeling of casting processes, and software development. He has published more than ten articles, won four scientific research awards, two software copyrights, and five patents.

JIANXIN ZHOU was born in Hunan, China, in 1975. He received the B.S., M.S., and Ph.D. degrees in materials processing engineering from the Huazhong University of Science and Technology, Wuhan, China. He is currently the Vice Director of the Department of Materials Processing, the Vice Director of the State Key Laboratory of Materials Processing and Die & Mould Technology, the Chief Professor of the Research Team of Intelligent Green Casting Technology and Application, the Head of the Research Team, InteCAST Software Center, Huazhong University of Science and Technology. He has published over 200 articles and two books. He has edited five proceedings in the conference. His main research interests include CAE technology, solidification, simulation, software development, and engineering application research, digital casting technology, such as process optimization design and production quality control. He won the Second Prize of the National Science and Technology Progress Award, in 2007 (No. 4), and in 2018 (No. 2), the 11th Hubei Youth Science and Technology Award, in 2013, the First National Foundry Industry Outstanding Young Talent Award, in 2015, the First Prize of the Cooperative Innovation Achievements (No. 1), in 2015, Individuals won the 2016 China-Industry-Research Cooperation Innovation Award, and 2011–2016 Chinese Mechanical Engineering Society Advanced Workers. He also won the First Prize of the Science and Technology Progress Award of Hubei Province, in 2017 (No. 1), the First Prize of the Science and Technology of China Machinery Industry, in 2017 (No. 1).